# Exploring the correlation between the spin-state configuration and the magnetic order in Co-substituted $BiFeO_3$

Koomok Lee,[1] Kei Shigematsu,[1,2] Hena Das,[1,2,3,*] and Masaki Azuma[1,2]

[1]*Laboratory for Materials and Structures, Tokyo Institute of Technology, 4259 Nagatsuta, Midori-ku, Yokohama, Kanagawa 226-8503, Japan*
[2]*Kanagawa Institute of Industrial Science and Technology, 705-1 Shimoimaizumi, Ebina 243-0435, Japan*
[3]*Tokyo Tech World Research Hub Initiative (WRHI), Institute of Innovative Research, Tokyo Institute of Technology, 4259 Nagatsuta, Midori-ku, Yokohama, Kanagawa 226-8503, Japan*

(Received 7 April 2022; accepted 18 May 2022; published 1 June 2022)

Co-substituted $BiFeO_3$ systems exhibit both ferroelectric and antiferromagnetic (AFM) orders with a considerably high electric polarization **P** and a modestly canted magnetization **M** and a cross coupling between them at room temperature. In the present study, employing first-principles calculations and Monte Carlo simulations, we unravel the microscopic interactions that contribute to stabilize this particular canted AFM order with **M**. Our results propose a correlation between the spin-state configuration of the trivalent $Co^{3+}$ ions and the energetics associated with the magnetic orders. Because of the complex interplay between the Hund's coupling ($J_H$) and crystal field splitting ($\Delta_{CF}$), the trivalent $Co^{3+}$ ions are known to exhibit three spin ($S$) configurations, namely low ($t_{2g}^6 \rightarrow S = 0$) spin (LS), intermediate ($t_{2g}^5 e_g^1 \rightarrow S = 1$) spin (IS), and high ($t_{2g}^4 e_g^2 \rightarrow S = 2$) spin (HS). We observe electron correlation induced LS $\rightarrow$ HS state transition, which implies a close competition among these spin states in the $R3c$ polar structure. Moreover, our detailed analysis points towards the formation of heterogeneous spin-state configuration at room temperature. While the LS state configuration was not observed to exhibit any particular tendency to stabilize the canted AFM phase, the HS state tends to strongly favor the formation of this desired magnetic order. On the other hand, interestingly, the formation of finite fraction of the IS state can contribute to enhance the magnitude of **M**. Our investigation is expected to initiate further quest for appropriate magnetic substitutes to ensure enhanced functionalities of the system.

DOI: 10.1103/PhysRevMaterials.6.064401

## I. INTRODUCTION

Bismuth ferrite ($BiFeO_3$) is one of the most extensively studied multiferroics, which exhibits distinct ferroelectric (FE) and antiferromagnetic (AFM) orders as well as a strong coupling between the two at room temperature [1–6]. The system crystallizes in the $R3c$ structure [Fig. 1(a)] below ~1100 K [4] resulting in considerable electric polarization $P \sim 100\ \mu C/cm^2$ along the crystallographic $(001)_H$ direction owing to the off-centric displacement of the bismuth ($Bi^{3+}$) ions [7]. The AFM order below ~640 K [8,9], on the other hand, is governed by the mutual microscopic magnetic interactions of the ferric ($Fe^{3+}$) ions. The magnetic order in $BiFeO_3$ is complex in nature [10–13]. Competing magnetic interactions like isotropic symmetric exchange, antisymmetric Dzyaloshinskii-Moriya [14,15] exchange, and single ion magnetic anisotropy of the ferric ions, lead to the formation of magnetic orders like the (1) collinear G-type AFM order and (2) long period cycloidal order. The formation of the latter order results in the cancellation of the modestly canted magnetization (**M**) of the former order. $BiFeO_3$ exhibits a cycloidal order with $\lambda \sim 62$ nm period [10] propagating along the crystallographic $[110]_H$ direction below Néel temperature ($T_N \sim 640$ K), suppressing ferromagnetic (FM) order of the canted spins, thereby leading to the suppression of **M**. Numerous researches have been conducted so far to discover effective ways of manipulation of these microscopic magnetic interactions to control the interphase transitions. Chemical substitution [16–20], application of epitaxial strain/pressure [21–25], electric field [26,27], and optical stimulation [28,29], are some of the noteworthy techniques in this regard.

As for chemical substitution, various attempts have been made to stabilize the canted AFM phase by partially substituting $Fe^{3+}$ ions with other transition metal (TM) ions [30]. $BiFe_{1-x}Co_xO_3$ systems, obtained by the substitution of $Fe^{3+}$ ions with trivalent cobalt ions, was found to be highly effective in this regard [31–38]. Neutron powder diffraction measurements and Mössbauer spectroscopy reported magnetic phase transition from low-temperature cycloidal to canted collinear G-type phase at ~120 K, resulting in a weak ferromagnetic behavior with $M \sim 0.02-0.06\ \mu_B$ per magnetic ion perpendicular to the electric polarization at room temperature [32–38]. Magnetization reversal by electric field was demonstrated in thin film samples [34,39–41]. The trivalent cobalt ions $Co^{3+}$ in octahedral oxygen coordination can exhibit various spin-state configurations, such as low ($t_{2g}^6 \rightarrow S = 0$) spin (LS), intermediate ($t_{2g}^5 e_g^1 \rightarrow S = 1$) spin (IS), and high ($t_{2g}^4 e_g^2 \rightarrow S = 2$) spin (HS) (here $S$ represents the spin of $Co^{3+}$ ions). Moreover, on account of the complex interplay between the Hund's coupling ($J_H$) and crystal field splitting ($\Delta_{CF}$), spin crossover transitions are common phenomena in the

*das.h.aa@m.titech.ac.jp

 

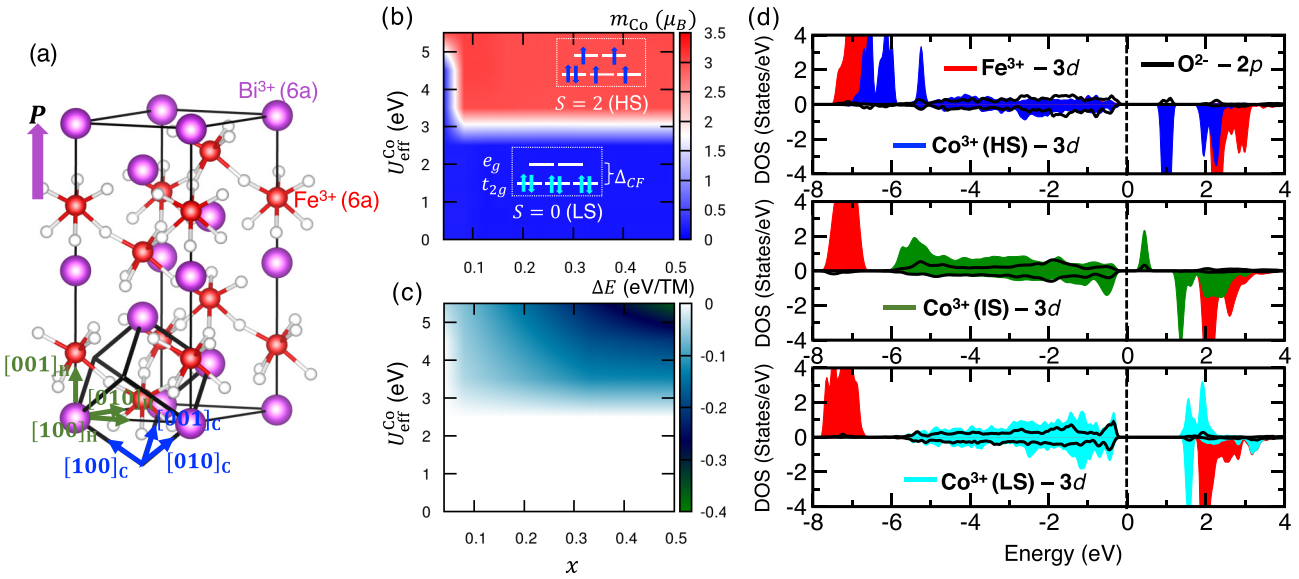


FIG. 1. (a) Polar $R3c$ crystal structure of $BiFeO_3$ consisting of out-of-phase $FeO_6$ octahedra rotation around cubic $Pm\bar{3}m$ $[111]_C$ axis and polar displacements of Bi ion along the same direction. The electric polarization is directed along the hexagonal $[001]_H$ (cubic $[111]_C$) axis. The trivalent Co ions substitute trivalent Fe ions at the $6a$ positions. [(b), (c)] Calculated magnetic moment of the Co spins and relative energy ($\Delta E(x, U_{\text{eff}}^{\text{Co}}) = E_{\text{GS}}(x, U_{\text{eff}}^{\text{Co}}) - E_{\text{LS}}(x, U_{\text{eff}}^{\text{Co}})$, where $E_{\text{GS}}(x, U_{\text{eff}}^{\text{Co}})$ and $E_{\text{LS}}(x, U_{\text{eff}}^{\text{Co}})$ denote the total energy of the ground state and low spin-state configuration, respectively) of the ground-state spin configuration as functions of $U_{\text{eff}}^{\text{Co}}$ and $x$. Insets show the occupancy of the $3d$ orbitals corresponding to low-spin (LS) ($S = 0$) and high-spin (HS) ($S = 2$) configurations. (c) Calculated density of states (DOS) of the HS (upper panel), IS (middle panel), and LS (lower panel) configurations for $U_{\text{eff}}^{\text{Co}} = 3.5$ eV.

compounds consisting of trivalent cobalt ions [42], leading to the emergence of fascinating novel phases in the proximity of the spin crossover transitions [43]. Notably, when $J_H \gg \Delta_{\text{CF}}$, the energy gain due to the FM Hund's exchange tends to stabilize the HS state configuration. Conversely, formation of the LS configuration is expected to be realized when $\Delta_{\text{CF}} \gg J_H$. However, when these two energy scales are at par with each other, the likelihood of spin crossover transitions in the system becomes high and the nature of such transitions are contingent upon subtle changes in the crystal structure brought about by controlling external factors, such as temperature, magnetic field, carrier doping, pressure, and strain. A typical example is $LaCoO_3$ [42,43]. Accordingly, the spin state of the substituted $Co^{3+}$ ions in $BiFe_{1-x}Co_xO_3$ is still ambiguous. While various experimental observations and the theoretical findings in $BiFe_{1-x}Co_xO_3$ ($x \leqslant 0.2$) have indicated the formation of LS state [31–34], a LS $\rightarrow$ IS state transition at around $T_S \sim 150$ K was also reported [38,44]. On the other hand, the measured Co $2p$ x-ray absorption spectra (XAS) of the $BiFe_{1-x}Co_xO_3$ ($0 < x \leqslant 0.3$) thin films indicated the formation of HS state at room temperature [18]. Incidentally, the value of $T_S$ is also close to the cycloidal to canted G-type phase transition temperature $T^*$, indicating a possible correlation between the spin-state configurations and the magnetic orders, which, to the best of our knowledge, is yet to be explored.

In the present study, employing first-principles density functional theory (DFT) + U method we showed that the spin state of $Co^{3+}$ ions in $BiFe_{1-x}Co_xO_3$ ($0 \leqslant x \leqslant 0.5$) compositions is not uniquely defined. Instead, there is a distinct possibility of spin crossover transitions depending on the influence of the external factors or structural particulars of the system. This is indicated by the electron correlation induced LS $\rightarrow$ HS state transitions, a phenomenon, which we have endeavored to elucidate in this study. In fact, by comparative analysis with the experimental data at room temperature, we propose a likelihood of coexistence of multiple spin-state configurations at room temperature. The HS state configurations exhibit strong spin-orbit coupling with high in-plane ($\{001\}_H$) magnetic anisotropy, which is order of magnitude higher than that of the $Fe^{3+}$ ions. Monte Carlo simulations at finite temperature indicate that increase in the fraction of the HS spin state increases the stability of the canted G-type magnetic order. Here, neither the HS nor the LS configuration leads to a considerable enhancement in **M**. However, the formation of IS state configuration with partially filled $e_g$ orbitals indicates a possibility of a significant enhancement in **M**. Our findings are expected to stimulate further research to determine the spin state of the substituted cobalt ions and to induce enhancement in functionality.

## II. COMPUTATIONAL DETAILS

We performed first-principles calculations by employing density functional theory (DFT) + U method [45] using the Perdew-Burke-Ernzerhof (PBE) form of exchange correlation functional [46] and the projector augmented plane- wave basis-based method as implemented in the VASP [47,48]. The cation ordered and the quasirandom structures [special quasirandom structures (SQS)] [49,50] of the $BiFe_{1-x}Co_xO_3$ compositions were optimized by employing a convergence criteria of 0.001 eV/Å for the Hellmann-Feynman forces on each atom and a kinetic energy cut-off value of 500 eV. Adequate $k$-point mesh was employed depending on the cell size and the symmetry of the structures. In the present study,

we have used rotationally invariant approach of DFT + U method [45] with an effective Hubbard parameter of value $U_{\text{eff}}^{\text{Fe}} = U^{\text{Fe}} - J_H^{\text{Fe}} = 4.5$ eV for the Fe $3d$ orbitals, where $J_H^{\text{Fe}}$ denotes Hund's coupling. As the effective Hubbard $U_{\text{eff}}^{\text{Co}}$ at the Co $3d$ orbitals is expected to play a crucial role to determine the electron occupancy of the $3d$ states and hence the spin state, we conducted structural optimization and total energy calculations by considering a wide range of $U_{\text{eff}}^{\text{Co}}$. In order to estimate the strength of various symmetric isotropic exchange interactions between the magnetic ions we conducted total energy calculations considering various collinear spin configurations in the absence of the spin-orbit $(L - S)$ coupling. On the other hand, the values of single-ion-anisotropy parameters of each magnetic ions were estimated considering total energy of various collinear spin structures in the presence of $L - S$ coupling as implemented in VASP. We crosschecked the values of various magnetic parameters by employing DFT + U based linearized augmented plane-wave (LAPW) method as implemented in the Wien2k code [51,52] and considering PBE [46] form of exchange correlation functional. We performed calculations using Wien2k by considering a plane-wave cutoff of $RK_{\text{MAX}} = 7$. Also, we employed appropriate values of the effective Hubbard parameter and Monkhorst-Pack Γ centered $k$-point mesh [53] keeping a parity with the VASP calculations.

In order to investigate the stability of the magnetic order at finite temperature we conducted classical Monte Carlo (MC) simulations by employing METROPOLIS algorithms [54,55] with proper periodic boundary conditions as implemented in our group MC package. We calculated total energy $\xi(T)$ as a function of temperature $(T)$, for each value of $x$ and each set of magnetic parameters, by considering $N_{\text{MC}}$ MC steps for each temperature step and performing $N_{\text{ion}}$ spin flips, where $N_{\text{ion}}$ denotes total number of magnetic ions in the MC cell. In the process of each spin flip, a random rotation of the direction of the selected spin is introduced by maintaining a uniform probability distribution of the associated unit spin vector over the respective unit sphere. In order to detect the magnetic transitions we calculated specific heat as a function of temperature using

$$C_v(T) = \frac{\langle \xi(T)^2 \rangle - \langle \xi(T) \rangle^2}{k_B T^2} \tag{1}$$

where the angle bracket denotes thermal average. The net magnetization $\mathbf{M}$ as function of $T$ was calculated by using

$$M_\varrho = \frac{1}{N_{\text{ion}}} \sum_{i=1}^{N_{\text{ion}}} g \mu_B S_\varrho^i \tag{2}$$

where, $\varrho = 1, 2, 3$ represent component of $\mathbf{M}$ along the Cartesian axes $x$, $y$, and $z$, respectively. $\mu_B$ is the Bohr magneton and $g \approx 2$ denotes the gyromagnetic ratio.

## III. RESULTS AND DISCUSSIONS

### A. Effect of electron correlation

The trigonal ground-state crystal structure $R3c$ of $BiFeO_3$ results from the out-of-phase octahedral rotations $(a^-a^-a^-)$ of the $FeO_6$ octahedra $[R_5^-(a, a, a) \rightarrow R\bar{3}c]$ around the cubic $Pm\bar{3}m$ $[111]_c$ axis and the polar displacements of the Bi ions $[\Gamma_4^-(a, a, a) \rightarrow R3m]$ along the same direction, leading to an electric polarization (**P**) [see Fig. 1(a)]. On the other hand, driven by the $\Gamma_4^-(0, 0, a)$ polar displacements of the Bi ions, the tetragonal $P4mm$ phase was reported to form under the application of appropriate epitaxial strain [56–59]. Our total energy calculations using an effective Hubbard parameter $U_{\text{eff}}^{\text{Fe}} = U^{\text{Fe}} - J_H^{\text{Fe}} = 4.5$ eV at the Fe $3d$ states and G-type AFM order between $S = \frac{5}{2}$ spins, show that the $P4mm$ is only 16 meV/f.u. higher in energy than the $R3c$ phase. We, therefore, investigated $BiFe_{1-x}Co_xO_3$ compositions, considering both the polar $R3c$ and $P4mm$ structures by substituting the Fe ions at the $6a$ and $1b$ Wyckoff positions, respectively. Notably, one of the end members, $BiCoO_3$, also crystallizes in the $P4mm$ structure, forming $CoO_5$ pyramidal coordination with high spin state of $Co^{3+}$ [60,61]. Morphotropic phase transitions may significantly contribute to manipulate the magnetic order.

We investigated both cation ordered and disordered configurations by constructing special quasirandom structures (SQS) [49,50] employing the $2 \times 2 \times 1$ supercell of the hexagonal $R3c$ structure. The supercell has 120 atoms and approximates disordered solid solutions of $BiFe_{1-x}Co_xO_3$. We incorporated these SQS structures because no clear evidence of cation ordering from experimental measurements has so far been detected. The technique to generate these structures are based on the close reproduction of the perfectly random network for the first few shells around a given site, as implemented in the alloy theoretic automated toolkit (ATAT) [50]. Notably, this technique has been successfully used to model atomic disordered configurations in various real materials [62,63].

While the high spin state of $Fe^{3+}$ ions is robust and relatively independent of the electron correlation factor $U_{\text{eff}}^{\text{Fe}}$, the effective Hubbard parameter $(U_{\text{eff}}^{\text{Co}} = U^{\text{Co}} - J_H^{\text{Co}})$ at the trivalent Co $3d$ orbitals can play a crucial role in the determination of the $d$ orbital occupancy and hence on the spin-state configuration, as was reported in $LaCoO_3$ [64,65]. In reviewing the end member $BiCoO_3$, we observed that irrespective of the value of $U_{\text{eff}}^{\text{Co}}$, $P4mm$ structure with HS configuration is much lower in energy compared to the $R3c$ phase (see Fig. S1 in the Supplemental Material [66]), which is in good agreement with various reports [60,61]. $BiCoO_3$ exhibits HS → LS state transition under the application of pressure [67]. It is also worth noting that the $R3c$ phase exhibits electron correlation driven LS → HS state transition in contrast to the $LaCoO_3$ system where the HS state is much higher in energy and the electron correlation induces LS → IS state transitions [64]. We, therefore, first explored the effect of electron correlation in the stability of the Co spin state in $BiFe_{1-x}Co_xO_3$ compositions $(0 < x \leqslant 0.5)$. We conducted full structural optimization of the cation ordered and constructed SQS structures employing 0.001 eV/Å convergence criteria of the Hellmann-Feynman forces within $0 \leqslant U_{\text{eff}}^{\text{Co}} \leqslant 5.5$ eV parameter space and G-type AFM order between the magnetic ions. We initiated the calculations considering various values of local magnetic moment at the Co site to determine the total energy associated with various spin states. Irrespective of the value of $U_{\text{eff}}^{\text{Co}}$ and $x$,

within $0 < x \leqslant 0.5$, the Fe/Co ordered configurations were found to be close in energy ($\Delta E \sim 2-3$ meV), indicating feasibility of formation of cation disordered structures at finite temperature.

We calculated and analyzed various properties indicative of spin crossover transitions [43], such as (1) the change in the average magnetic moment ($m_{\mathrm{Co}}$), (2) modulation of volume and lattice parameters, and (3) electronic structures. Figure 1(b) shows calculated modulation of $m_{\mathrm{Co}}$ as functions of $x$ and $U_{\mathrm{eff}}^{\mathrm{Co}}$ corresponding to the respective ground-state spin configurations in $R3c$ structure. $R3c \rightarrow P4mm$ phase transition was observed at around $x = 0.5$ for $U_{\mathrm{eff}}^{\mathrm{Co}} = 3.5$ eV, close to the experimentally determined transition point of $x \sim 0.4$ [68]. We did not observe any intermediate monoclinic phase as was reported experimentally [31,68]. For low cobalt concentration ($x \leqslant 0.08$) region, our results show that the system tends to configure in the LS state. However, for higher Co concentrations, our results show a change in $m_{\mathrm{Co}}$ from $\sim 0.2 \rightarrow \sim 3.01\ \mu_B$ at around $U_{\mathrm{eff}}^{\mathrm{Co}} = 3.0$ eV, which corresponds to LS $\rightarrow$ HS transitions, similar to $BiCoO_3$. This phenomenon has been observed for both ordered and disordered configurations. The corresponding calculated relative energies ($\Delta E$) are shown in Fig. 1(c). The associated formation energies of various spin-state configurations having the formula

$$\Delta E_f = E[\mathrm{BiFe}_{1-x}\mathrm{Co}_x\mathrm{O}_3] - (1-x)E[\mathrm{BFO}] - xE[\mathrm{BCO}] \tag{3}$$

imply the formation of solid solution between $BiFeO_3$ and $BiCoO_3$ $R3c$ phases (see Fig. S2 in the Supplemental Material [66]). Here, $E$[BFO] and $E$[BCO] represent the internal energies of the G-type AFM ordered $R3c$ structures of the $BiFeO_3$ (BFO) and $BiCoO_3$ (BCO) end members, respectively.

Figure 1(d) shows the calculated density of states (DOS) corresponding to the HS (upper panel) and LS (lower panel) state configurations at $x = \frac{1}{6}$ and for $U_{\mathrm{eff}}^{\mathrm{Co}} = 3.5$ eV. We obtained an insulating solution for the entire range of $U_{\mathrm{eff}}^{\mathrm{Co}}$ and $x$. Similar to the parent system $BiFeO_3$, the majority spin channel of Fe $3d$ states is completely occupied, while the minority spin channel is almost empty, forming 3+ oxidation state. The magnetic moment of Fe ions $\sim 4.2\,\mu_B$. In case of the LS state configuration of the cobalt ions with $m_{Co} \sim 0.2\ \mu_B$, spin pairs are formed in the completely filled $t_{2g}$ manifold, leaving the $e_g$ manifold almost empty, confirming the formation of LS 3+ oxidation state of Co ($t_{2g}^6 e_g^0$). As was also observed in $Co_3O_4$ [69], a strong hybridization with the oxygen $2p$ states leads to $m_{Co} \sim 0.2\ \mu_B$. On the other hand, the spin-state configuration with $m_{Co} \sim 3.01\ \mu_B$ exhibits completely filled majority $3d$ channel and partially occupied minority $t_{2g}$ states, both strongly hybridized with oxygen $2p$ orbitals. This was observed also for the HS state configuration of $BiCoO_3$ [70]. Therefore $m_{Co} \sim 3.01\ \mu_B$ state corresponds to HS 3+ oxidation state of Co ($t_{2g}^4 e_g^2$). This is in extremely close agreement with the experimentally determined magnetic moment of $Co^{3+}$ ions, $\sim 2.82\,\mu_B$ [44], in $BiFe_{1-x}Co_xO_3$ at room temperature. In this system, an increase in $U_{\mathrm{eff}}^{\mathrm{Co}}$, therefore, destabilizes the spin pairing at the $t_{2g}$ orbitals in the LS state and stabilizes the HS state due to the enhancement of the ferromagnetic Hund's exchange energy. Formation of a fraction of IS state, however, was found to be associated with higher energy compared to the ground state [see Fig. 2(b)].

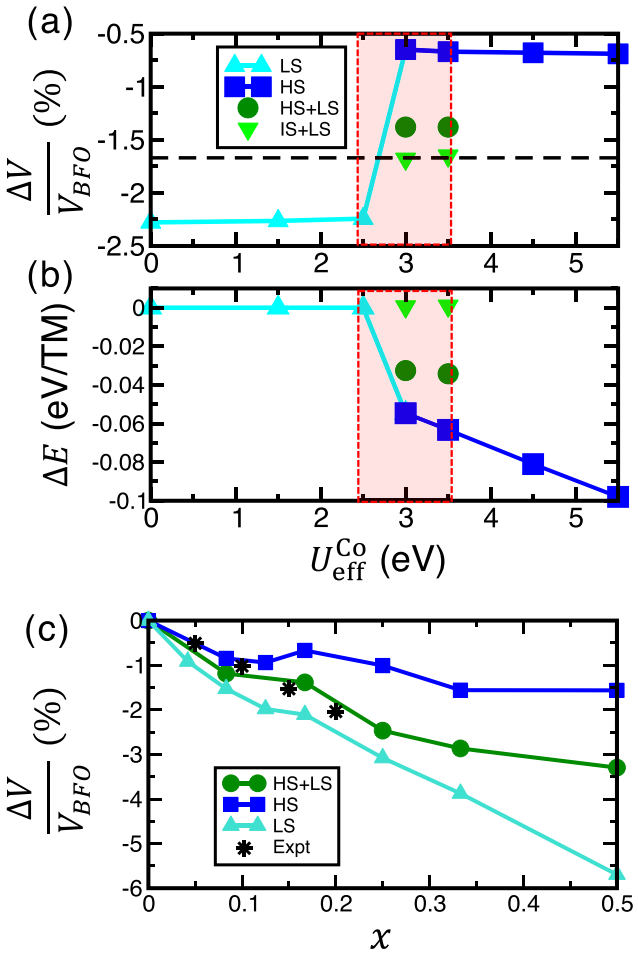


FIG. 2. [(a), (b)] Calculated reduction of the volume ($\frac{\Delta V}{V_{\mathrm{BFO}}}$) with respect to parent compound $BiFeO_3$ and relative energy ($\Delta E$) of various spin-state configurations of $BiFe_{5/6}Co_{1/6}O_3$ composition as a function of $U_{\mathrm{eff}}^{\mathrm{Co}}$. The experimental value of $\frac{\Delta V}{V_{\mathrm{BFO}}}$ (Ref. [33]) is denoted by dashed line. (c) Calculated $\frac{\Delta V}{V_{\mathrm{BFO}}}$ of $BiFe_{1-x}Co_xO_3$ compositions as functions of $x$ and Co spin configuration for $U_{\mathrm{eff}}^{\mathrm{Co}} = 3.5$ eV. The experimental data from Ref. [33] are shown with black stars. $V_{\mathrm{BFO}}$ represents the volume of the parent compound $BiFeO_3$.

As shown in Fig. 1(d) (middle panel), IS state of $Co^{3+}$ corresponds to $t_{2g}^5 e_g^1$ electronic structure with a magnetic moment of $m_{Co} \sim 1.9\ \mu_B$.

As expected, the volume of the $CoO_6$ octahedra gradually decreases as one moves from HS $\rightarrow$ IS $\rightarrow$ LS state configuration. Therefore, a magneto-volume effect is expected to be observed at the spin crossover transition, as shown for $x = \frac{1}{6}$ in Figs. 2(a) and 2(b). Interestingly, detailed comparative analysis of the first-principles data and the experimentally observed volume reduction phenomena at room temperature indicates the crystallization of multiple spin states associated to $U_{\mathrm{eff}}^{\mathrm{Co}} = 3.5$ eV, as depicted in Fig. 2(c). Further investigations around electron correlation induced spin-state crossover transition window $2.5 \leqslant U_{\mathrm{eff}}^{\mathrm{Co}} \leqslant 3.5$ eV for $x = \frac{1}{6}$ [see Fig. 2(a)] also raise the possibility of formation of multiple spin-state configurations at room temperature. The modulation of average (TM)-O bond lengths and volume of the $(TM)O_6$ octahedra as functions of spin states and $x$

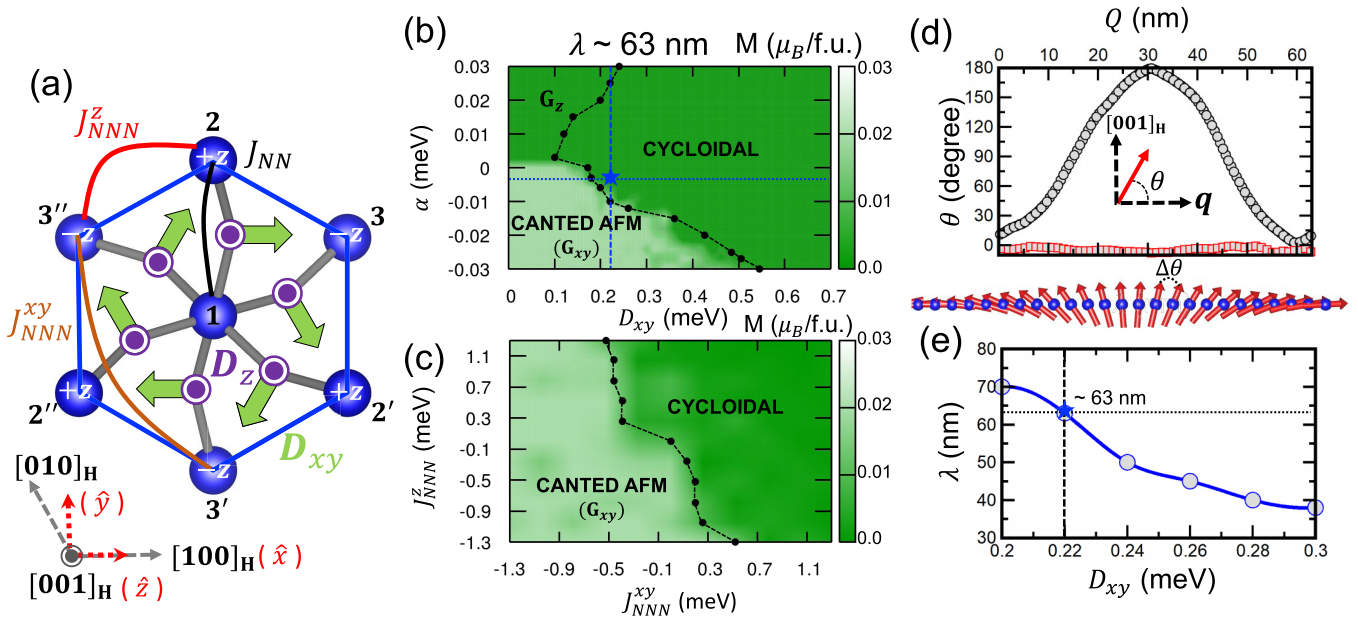


FIG. 3. (a) Symmetric isotropic and antisymmetric anisotropic DM interactions between the magnetic ions (depicted with blue spheres). The NN DM vector pattern of each magnetic ion (marked by 1) is illustrated in the Cartesian coordinate. Each NN DM vector consists of two components: (1) transverse component $\mathbf{D}_{xy}$ (denoted by green arrows) in the $xy$ ($\{001\}_H$) plane induced by the $a^-a^-a^-$ ($R_5^-$) displacements and (2) longitudinal component along the $\hat{z}$ ($[001]_H$) axis $\mathbf{D}_z$ (denoted by purple dot mark) induced by the $\Gamma_4^-(a,a,a)$ polar displacements. The atoms $2, 2', 2''$ $(3, 3', 3'')$ represent the NN along the positive (negative) $\hat{z}$ axis. (b) Calculated net magnetization $\mathbf{M}$ of the most stable magnetic state as functions of $\mathbf{D}_{xy}$ and SIA parameter $\alpha$ at 5 K. The magnetic transitions from G-type AFM to cycloidal phase are denoted by solid-black circles. $G_{xy}$ and $G_z$ represent G-type order of spins oriented in the $xy$ ($\{001\}_H$) plane and along the $\hat{z}$ ($[001]_H$) axis, respectively. $G_{xy}$ allows canted spin components induced by $\mathbf{D}_z$ ordered in FM pattern leading to a nonzero value of $\mathbf{M}$. (c) Calculated net magnetization $\mathbf{M}$ of the most stable magnetic state as functions of NNN symmetric exchange interactions at 5 K. (d) Calculated angle ($\theta$) of the spins with respect to the propagation vector $\mathbf{q}$. The periodic modulation of $\theta$ represents cycloidal order, while $\theta \sim 0$ denotes $G_{xy}$ order. (e) Estimated period of cycloidal modulation of spins $\lambda$ as a function of $D_{xy}$ for DFT estimated values of SE interactions, SIA parameter $\alpha$ and $D_z = 0.08$ meV. Our results lead to 63 nm cycloidal period for $D_{xy} \sim 0.22$ meV [as illustrated by star in (b) and (e)].

are shown in Fig. S3 in the Supplemental Material [66] for $U_{\text{eff}}^{\text{Co}} = 3.5$ eV. Driven by the $\Gamma_4^-(a,a,a)$ polar distortion, each $FeO_6$ octahedron exhibits three long and short Fe-O bond formations. In comparison, $CoO_6$ octahedra with HS state configuration having almost similar volume ($\frac{\Delta V_{CoO_6}}{V_{FeO_6}} \sim -3\%$) are strongly distorted. This effect gets reduced in LS configuration forming almost regular $CoO_6$ octahedra with significant reduction in volume of $\frac{\Delta V_{CoO_6}}{V_{FeO_6}} \sim -10\%$. On the other hand, the IS configuration with $\frac{\Delta V_{CoO_6}}{V_{FeO_6}} \sim -5\%$ shows weak local Jahn-Teller (JT) distortion. Our detailed analysis of the various spin-state configurations is expected to contribute to the detection of any possible spin crossover transition in $BiFe_{1-x}Co_xO_3$ systems.

### B. Magnetic order

To explore the influence of the $Co^{3+}$ spin-state configuration on the resultant magnetic order, we conducted Monte Carlo simulations at finite temperature employing a spin model consisting of symmetric isotropic exchange (SE) and antisymmetric Dzyaloshinskii-Moriya (DM) exchange interactions between the magnetic ions and their single ion anisotropy (SIA). The model is represented as

$$H = H_1 + H' \tag{4}$$

where $H_1$ represents the spin model associated with $Fe^{3+}$ ($S = \frac{5}{2}$) spins and $H'$ denotes variation due to the trivalent cobalt substitution. $H_1$ can be defined as

$$H_1 = H_{\text{SE}} + H_{\text{DM}} + H_{\text{SIA}} \tag{5}$$

where

$$H_{\text{SE}} = \sum_{\langle i,j\rangle_{\text{NN}}} J_{\text{NN}} \mathbf{S}_i \cdot \mathbf{S}_j + \sum_{\langle i,j\rangle_{\text{NNN}_{|z}}} J^z_{\text{NNN}} \mathbf{S}_i \cdot \mathbf{S}_j + \sum_{\langle i,j\rangle_{\text{NNN}_{|xy}}} J^{xy}_{\text{NNN}} \mathbf{S}_i \cdot \mathbf{S}_j, \tag{6}$$

which includes nearest-neighbor (NN) superexchange interactions $J_{\text{NN}}$ between Fe spins with six coordination number and the next-nearest-neighbor (NNN) out-of-plane ($J^z_{\text{NNN}}$) and in-plane ($J^{xy}_{\text{NNN}}$) magnetic interactions, as depicted in Fig. 3(a). The $\langle i,j\rangle_{\text{NN}}$ denotes the sum over NN Fe-Fe pairs along the crystallographic $[001]_H$ ($\hat{z}$) axis. Whereas the sums $\langle i,j\rangle_{\text{NNN}_{|z}}$ and $\langle i,j\rangle_{\text{NNN}_{|xy}}$ go over NNN Fe-Fe pairs along the $[001]_H$ ($\hat{z}$) axis and in the $\{001\}_H$ ($xy$) plane, respectively. Every spin pair was counted once. As in the $3d$ transition metal oxide, the strength of the DM interactions are expected to be order of magnitude weaker than the SE counterpart [71]. We, therefore, considered only NN interactions with the corresponding

energy term,

$$H_{\rm DM} = \sum_{\langle i,j\rangle_{\rm NN}} \mathbf{D}_{z_{i,j}} \cdot \mathbf{S}_i \times \mathbf{S}_j + \sum_{\langle i,j\rangle_{\rm NN}} \mathbf{D}_{xy_{i,j}} \cdot \mathbf{S}_i \times \mathbf{S}_j. \quad (7)$$

While the NN transverse component $\mathbf{D}_{xy_{i,j}}$ induced by the polar distortions tends to create cycloidal modulation in the G-type AFM order of the Fe spins and determines the period ($\lambda$), the longitudinal component induced by the $a^-a^-a^-$ octahedral rotations $\mathbf{D}_{z_{i,j}}$ cant the spins ordered in FM pattern. The NN DM vectors around each magnetic ion are depicted in Fig. 3(a). The third energy contribution $H_{\rm SIA}$ arises from the magnetic anisotropy of the $Fe^{3+}$ ions, defined as

$$H_{\rm SIA} = \sum_i \mathbf{S}_i \cdot \hat{\tau} \cdot \mathbf{S}_i. \quad (8)$$

In the $R3c$ hexagonal symmetry, the SIA tensor $\hat{\tau}$ consists of nonzero diagonal components with $\tau_{xx} = \tau_{yy} = \alpha$ and $\tau_{zz} = -2\alpha$ [72]. The negative and the positive values of $\alpha$ tend to align the Fe spins in the $\{001\}_H$ plane and along the $[001]_H$ axis, respectively.

As expected, the half-filled electronic configuration of Fe ions ($3d^5 \rightarrow t_{2g}^3 e_g^2$) gives rise to strong AFM SE interaction between NN Fe ions with a magnitude of $J_{\rm NN} \sim 6.5$ meV for $U_{\rm eff}^{\rm Fe} = 4.5$ eV. The NNN Fe-Fe interactions are also AFM in nature and order of magnitude weaker than $J_{\rm NN}$. The average strength of NNN Fe-Fe interaction is $J_{\rm NNN} = (J^z_{\rm NNN} + J^{xy}_{\rm NNN})/2 \sim 0.3$ meV. These antiferromagnetically coupled Fe spins exhibit weak magnetic anisotropy with $\alpha \sim -0.003$ meV, driven by the weak spin-orbit coupling induced by the Fe-3$d$-O-2$p$ hybridization. We estimated the value of $\alpha$ from $\alpha = \frac{E_{[001]_H} - E_{[001]_H}}{3S^2}$, where $E_{\{001\}_H}$ and $E_{[001]_H}$ denote the total energy corresponding to the spin configurations oriented in the $xy$ ($\{001\}_H$) plane and along the $\hat{z}$ ($[001]_H$) axis, respectively. The calculated orbital moment at the Fe site $m_o \sim 0.02\ \mu_B$. We crosschecked the values of these parameters by employing DFT + U based linearized augmented plane-wave (LAPW) method as implemented in the Wien2k code [51,52] and considering PBE [46] form of exchange correlation functional. These estimated values of magnetic parameters of the parent compound are in close agreement with the previous theoretical [72,73] and experimental [74–76] studies. Here, the strong $J_{\rm NN}$ interactions drive the robust G-type magnetic order between Fe spins, where each Fe spin is aligned antiferromagnetically with its NN Fe spins. On the other hand, the weak magnetic interactions, $J_{\rm NNN}$, $\alpha$, and $\mathbf{D}_{ij} = \mathbf{D}_{xy_{i,j}} + \mathbf{D}_{z_{i,j}}$, create a competition between the various magnetic orders, in any one of which the system can stabilize itself. We, therefore, conducted MC simulations by varying the values of these weak interactions to identify the factors that enhance the stability of the collinear G-type order in the $xy$ ($\{001\}_H$) plane (phase-$G_{xy}$) with a canted in-plane FM component ($\mathbf{M}$) over the cycloidal order.

The MC simulations were performed considering $2\sqrt{2} \times n\sqrt{2} \times 2$ supercells of the pseudocubic structures with $\{n \in \mathbb{Z} \mid 30 \leqslant n \leqslant 120\}$ [72]. The increase in the $n$ value represents an increase in the cell size along the propagation vector of the cycloidal order ($\mathbf{q}$). We checked the energies of the cycloidal order in the $33 \lesssim Q \lesssim 133$ nm range of the cell size along the propagation vector $\mathbf{q}$. In addition, we also performed MC calculations with $8\sqrt{2} \times 8\sqrt{2} \times 8$ pseudocubic cells to determine the energy and net magnetization $\mathbf{M}$ of the collinear G-type order. Figures 3(b) and 3(c) show the results of MC calculations. The $G_{xy}$ phase is characterized by the AFM order parameter $\mathbf{L}_{G_{xy}}$ and magnetization $\mathbf{M}$ with

$$M \approx \frac{D_z}{(J_{\rm NN} + 2J_{\rm NNN})} m_\gamma \quad (9)$$

where $m_\gamma$ denotes the magnetic moment of the $Fe^{3+}$ ions. On the other hand, the cycloidal order can be defined by the modulation in spin $\Delta\theta$ [see Fig. 3(d)] as

$$\tan\Delta\theta \approx \frac{\sqrt{3}D_{xy}}{2(J_{\rm NN} - 3J_{\rm NNN})}. \quad (10)$$

Increase in the value of $D_{xy}$, in turn, increases $\Delta\theta$ and decreases the period $\lambda$. Here $\Delta\theta = 0$ represents either phase-$G_{xy}$ or phase-$G_z$. In the former case, the spins are arranged in the $xy$ ($\{001_H\}$) plane with $\theta = 0$ or $\pi$, as defined in Fig. 3(d). In the latter, the spins are aligned along $\hat{z}$ ($[001]_H$) axis with $\theta = \frac{\pi}{2}$ or $\frac{3\pi}{2}$ and $\mathbf{M} = 0$ by symmetry.

As shown in Fig. 3(b), magnetic phase transition from the canted $G_{xy} \rightarrow$ cycloidal order occurs at around $D_{xy} \sim 0.18$ meV corresponding to the DFT estimated values of SE interactions and SIA. A cycloidal order with period ~63 nm, as observed from experimental measurements [10], gets stabilized for $D_{xy} \sim 0.22$ meV, as shown in Figs. 3(d) and 3(e). On the other hand, in the $G_{xy}$ phase, a net magnetization of value $M \sim 0.03\ \mu_B$/Fe, at par with experiment, develops for $D_z \sim 0.08$ meV (see Fig. S4 in the Supplemental Material [66]). The estimated strengths of DM interactions of $BiFeO_3$ employing the hybrid technique of first-principles calculations and MC simulations are in good agreement with previous experimental and theoretical reports [11,72,77–80]. The calculated Néel temperature $T_N \sim 605$ K also agrees well with experiment [8,9]. In Fig. 3(b), we observed that, while increase in the single-ion magnetic anisotropy enhances the stability of the $G_{xy}$ phase, increase in the transverse DM component $\mathbf{D}_{xy}$ energetically favor the cycloidal order. We also observed that the critical value of $\mathbf{D}^\gamma_{xy}$ at which the magnetic transition takes place varies quadratically with $\alpha$ in the parameter range of $-0.02 < \alpha \leqslant 0.0$ and linearly when $\alpha \leqslant -0.02$ (see Fig. S5 in the Supplemental Material [66]). Additionally, our results show that the reduction of magnetic frustration due to the AFM $J_{\rm NNN}$ also enhances the feasibility of formation of $G_{xy}$ [see Fig. 3(c)]. The uniaxial magnetic anisotropy, as shown in Fig. 3(b), indicates the formation of G-type ordered spins aligned along the $[001]_H$ direction, $G_z$, the symmetry of which does not allow any FM component. Our results indicate towards a possible stabilization of the $G_{xy}$ order with a net magnetization $\mathbf{M}$ by the substitution of $Fe^{3+}$ ions with appropriate magnetic ions having strong in-plane magnetic anisotropy and FM NNN interactions.

*LS configuration ($S = 0$).* The effect of the formation of LS state configuration in $BiFe_{1-x}Co_xO_3$ systems was simulated by the mere substitution of the Fe spins with nonmagnetic ions in the $H_1$ model. Figure 4(a) shows the results of MC calculations for $0 < x \leqslant 0.4$. In these calculations, we considered the estimated magnetic parameters of the parent compound, which stabilize the Cycloidal order with $\lambda = 63$ nm. The key

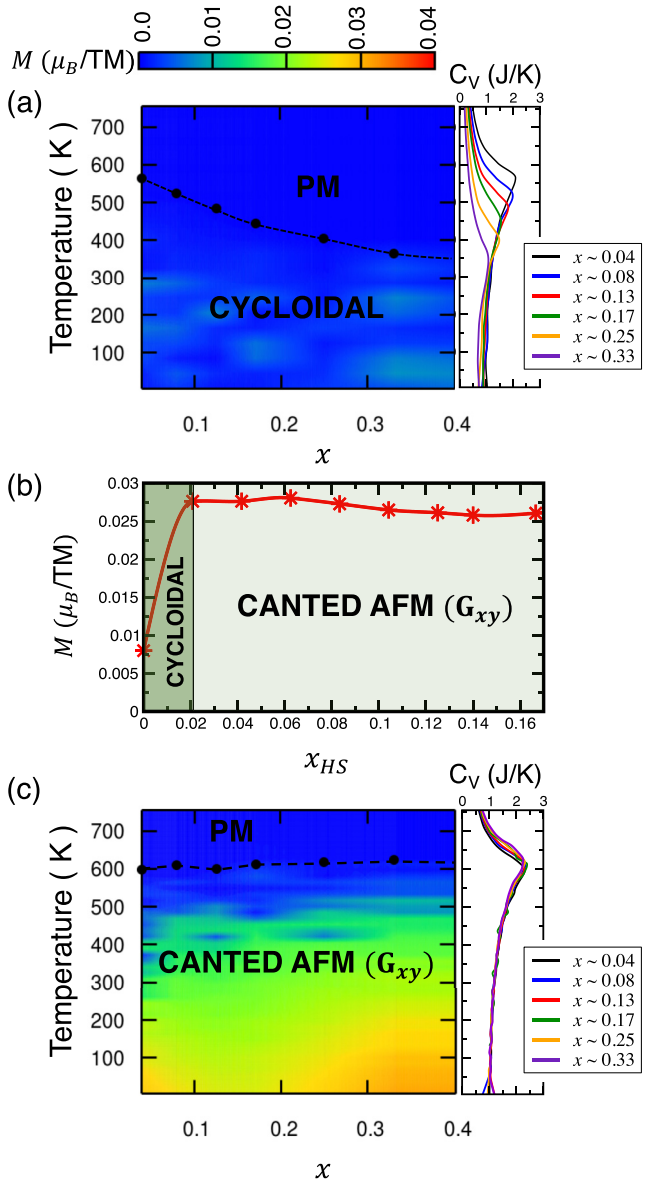


FIG. 4. Calculated net magnetization $M$ and specific heat of $BiFe_{1-x}Co_xO_3$ systems as functions of $x$ and temperature ($T$). (a) Corresponds to the results of MC simulations for the LS ($S = 0$) configurations. (b) Calculated $M$ as a function of the fraction of HS state $x_{\rm HS}$ for the lowest energy magnetic configuration at 5 K. These results correspond to $x = x_{\rm LS} + x_{\rm HS} = \frac{1}{6}$, where $x_{\rm LS}$ denotes fraction of LS state. (c) Calculated $M$ and specific heat as functions of $x$ and temperature ($T$) for the HS state configuration.

observation is that, with the gradual increase in the cobalt concentration, the system tends to form cycloidal order with a gradual decrease in $T_N$. The gradual decrease in $T_N$ is associated with a loss of the magnetic coordination caused by the decrease in Fe concentration. We did not observe any trace of a second magnetic phase transition as was indicated by the experiment [33,35] with the increase in temperature. In this model, the effect of the volume reduction and the hybridization of the Co-3$d$ orbitals with the O-2$p$, which can induce subtle changes in the magnetic interactions and affect the stability of magnetic orders, were not taken into consideration. We found that the reduction of volume by ∼2% at $x = \frac{1}{6}$ leads to a slight increase in $J_{\rm NN}$ ($\Delta J_{\rm NN} \sim 0.4$ meV) and a negligible change in $J_{\rm NNN}$ ($\Delta J_{\rm NNN} \sim 0.01$ meV) retaining weak in-plane magnetic anisotropy of the Fe spins. Accordingly, the strength of the DM interactions are also expected to be affected. The mere increase in $J_{\rm NN}$ was also found to stabilize the cycloidal order below $T_N \sim 485$ K. The formation of the LS state, therefore, is not associated with any dominating magnetic interaction that can unambiguously ensure the stabilization of the canted AFM order over the Cycloidal order.

*HS configuration ($S = 2$).* In order to conduct a simulated study of the influence of the HS state on the magnetic order we introduced some additional energy terms in the $H_1$ model, defined as

$$H' = H'_{\rm SE} + H'_{\rm DM} + H'_{\rm SIA}. \tag{11}$$

The key observation is that the HS state configuration exhibits strong $L - S$ coupling with the orbital moment $m_o^{\rm HS} \sim 0.18\ \mu_B$, order of magnitude higher than that of the LS configuration ($m_o^{\rm LS} \sim 0.04\ \mu_B$) and Fe ions ($m_o \sim 0.02\ \mu_B$). This phenomenon leads to strong in-plane $xy$ ($\{001\}_H$) magnetic anisotropy with $\tau_{xx}^{\rm HS} \approx \tau_{yy}^{\rm HS} \approx -\tau_{zz}^{\rm HS}/2 = \alpha' \sim -0.11$ meV, *i.e.*, $\frac{\alpha'}{\alpha} \approx \frac{(m_o^{\rm HS})^2}{(m_o)^2}$. The corresponding energy contribution is given by

$$H'_{\rm SIA} = \sum_{i'} \mathbf{S}'_{i'} \cdot \hat{\tau}' \cdot \mathbf{S}'_{i'} \tag{12}$$

where $S' = 2$ corresponds to the HS state. The possibility of a nonzero off-diagonal component of SIA tensor $\hat{\tau}'$ getting induced by the local octahedral distortions was not taken into consideration in the present study. While we estimated the value of $\alpha'$ we considered the value of $\alpha$ same as in the parent compound and used $\alpha' = \frac{(E'_{\{001\}_H} - E'_{[001]_H})}{3x(S')^2} - \frac{(1-x)S^2}{x(S')^2}\alpha$, where $E'_{\{001\}_H}$ and $E'_{[001]_H}$ denote the total energy corresponding to the spin configurations oriented in the $xy$ ($\{001\}_H$) plane and along the $\hat{z}$ ($[001]_H$) axis, respectively. We evaluated $\alpha'$ for $x = \frac{1}{6}$. We crosschecked these values by conducting total energy calculations using Wien2K method by switching on the $L - S$ coupling corresponding exclusively to the magnetic ion whose SIA parameter was to be calculated. We introduced NN and NNN symmetric Co-Fe and Co-Co exchange interactions terms, given by

$$H'_{\rm SE} = \sum_{\langle i',j\rangle_{\rm NN}} J_{\rm NN}^{\rm Co\text{-}Fe} \mathbf{S}'_{i'} \cdot \mathbf{S}_j + \sum_{\langle i',j'\rangle_{\rm NN}} J_{\rm NN}^{\rm Co\text{-}Co} \mathbf{S}'_{i'} \cdot \mathbf{S}'_{j'} + \sum_{\langle i',j\rangle_{\rm NNN}} J_{\rm NNN}^{\rm Co\text{-}Fe} \mathbf{S}'_{i'} \cdot \mathbf{S}_j + \sum_{\langle i',j'\rangle_{\rm NNN}} J_{\rm NNN}^{\rm Co\text{-}Co} \mathbf{S}'_{i'} \cdot \mathbf{S}'_{j'} \tag{13}$$

where $J_{\rm NN}^{\rm Co\text{-}Fe}$ ($J_{\rm NN}^{\rm Co\text{-}Co}$) and $J_{\rm NNN}^{\rm Co\text{-}Fe}$ ($J_{\rm NNN}^{\rm Co\text{-}Co}$) represent NN and NNN Co-Fe (Co-Co) SE interactions, respectively. The $\langle i', j\rangle_{\rm NN}$ and $\langle i', j'\rangle_{\rm NN}$ denote the sum over NN Co-Fe and Co-Co pairs along the crystallographic $[001]_H$ axis, respectively. Whereas the sums $\langle i', j\rangle_{\rm NNN}$ and $\langle i', j'\rangle_{\rm NNN}$ go over NNN Co-Fe and Co-Co pairs, respectively. We counted every spin pair once. In order to simplify the model, we assumed $J_{\rm NN}^{\rm Co\text{-}Fe} \approx J_{\rm NN}^{\rm Co\text{-}Co} = J'_{\rm NN}$ and $J_{\rm NNN}^{\rm Co\text{-}Fe} \approx J_{\rm NNN}^{\rm Co\text{-}Co} = J'_{\rm NNN}$. Thus we incorporated the effective interactions of every Co ions with the magnetic ions in the NN and NNN shells of the cation disordered structures.

These interactions were found to be AFM in nature with a estimated strength of $J'_{\rm NN} \sim 9.9$ meV and $J'_{\rm NNN} \sim 0.5$ meV for $x = \frac{1}{6}$. The Fe-Fe interactions, $J_{\rm NN} \sim 6.6$ meV and $J_{\rm NNN} \sim 0.3$ meV, show slight modification compared to that of the parent compound. In the similar fashion, we incorporated the effective DM interactions by assuming $D_z^{\text{Co-Fe}} \approx D_z^{\text{Co-Co}} = D'_z$ and $D_{xy}^{\text{Co-Fe}} \approx D_{xy}^{\text{Co-Co}} = D'_{xy}$. The corresponding energy term is given by

$$H'_{\rm DM} = \sum_{\langle i',j\rangle_{\rm NN}} \mathbf{D}_{i',j}^{\text{Co - Fe}} \cdot \mathbf{S}'_{i'} \times \mathbf{S}_j + \sum_{\langle i',j'\rangle_{\rm NN}} \mathbf{D}_{i',j'}^{\text{Co - Co}} \cdot \mathbf{S}'_{i'} \times \mathbf{S}'_{j'}. \tag{14}$$

We used the same vector pattern of the DM interactions as depicted in Fig. 3(a).

The strength of $\mathbf{D}'$, like the SIA, is expected to be higher in magnitude compared to its Fe-Fe counterpart ($\mathbf{D}$ with $D_{xy} = 0.22$ meV and $D_z = 0.08$ meV). To develop a further insight in this direction, employing $H_1 + H'$ spin model, we conducted MC simulations by varying the value of $D'_{xy}$ using $\frac{D'_z}{D'_{xy}} = \frac{D_z}{D_{xy}} \sim 0.4$ relationship for the cation disordered structure where $x = \frac{1}{6}$ of the Fe spins are substituted by the Co spins ($S = 2$). Similar to the parent system, we considered $2\sqrt{2} \times n\sqrt{2} \times 2$ supercells of the pseudocubic structures with $\{n \in \mathbb{Z} | 10 \leqslant n \leqslant 120\}$. Our results show that, regardless of the high magnitude of $D'_{xy}$, even as high as $D'_{xy} = \frac{1}{2}J'_{\rm NN} \sim 5$ meV, the magnetic ions are invariably order in the canted AFM $G_{xy}$ pattern (see Fig. S6 in the Supplemental Material [66]). We therefore, next, performed MC simulations as a function of the fraction of HS state, $x_{\rm HS}$ ($x = x_{\rm HS} + x_{\rm LS} = \frac{1}{6}$), considering $D'_{xy} = \frac{m_o^{\rm HS}}{m_o} D_{xy}$ and $D'_z = \frac{m_o^{\rm HS}}{m_o} D_z$. Figure 4(b) shows that a small variation in the fraction of the HS state, for $x_{\rm HS} \geqslant 0.02$, also leads to the stabilization of the canted $G_{xy}$ phase over the cycloidal order with $M \sim 0.03$ $\mu_B$/TM. Interestingly, this calculated value of $M$ for $x = \frac{1}{6}$ is in very good agreement with the value obtained from the DFT calculation with $U_{\rm eff}^{\rm Co} = 3.5$ eV. This justifies the choice of the DM parameters developed through the MC simulations. Finally, employing these estimated magnetic parameters for $x = \frac{1}{6}$, the results as a function of $x$ show the formation of the canted AFM order for the whole cobalt concentration range ($0 < x \leqslant 0.5$) under the present study, as shown in Fig. 4(c). Notably, the $M$ and $T_N$ did not record any significant variation with the change in cobalt concentration. Thus, our investigations indicate that the substitution of the Fe ions with magnetic ions having high in-plane ($\{001\}_H$) magnetic anisotropy, can effectively stabilize the desirable canted AFM order.

*IS configuration ($S = 1$).* Our results indicate that, if IS state forms in the disordered structure a highly canted component of the Co spin having a value $\eta_{\rm IS} \sim 0.6$–$0.8$ $\mu_B$ is expected to be observed. This IS state also exhibits a strong $L - S$ coupling with an orbital moment $m_o^{\rm IS} \sim 0.2$ $\mu_B$. The canted component $\eta_{\rm IS}$ is an order of magnitude higher compared to its LS ($\eta_{\rm LS} \sim 0.02$–$0.06$ $\mu_B$) and HS ($\eta_{\rm HS} \sim 0.02$–$0.06$ $\mu_B$) state counterparts. We observe that $M \sim 0.03$ $\mu_B$/TM for both the LS and HS configurations and it remains almost unchanged with the variation of $x$ and $U_{\rm eff}^{\rm Co}$. The average of $M$ corresponding to various mixed spin-state configurations as functions of $x$ and $U_{\rm eff}^{\rm Co}$, as summarized in Fig. 5, shows

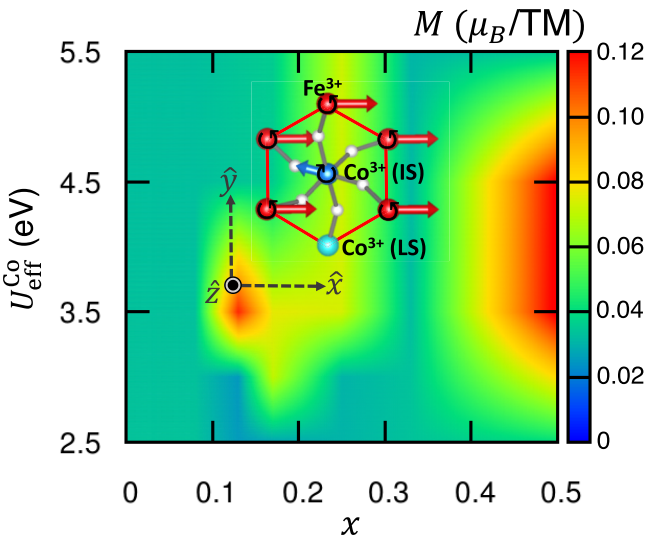


FIG. 5. DFT calculated average magnetization $M$ of the mixed spin-state configurations as functions of $x$ and $U_{\rm eff}^{\rm Co}$. Inset shows canted $G_{xy}$ configuration of $Co^{3+}$(IS)-$Fe_5^{3+}Co^{3+}$(LS) cluster in the disordered structure for $x = \frac{1}{6}$, as obtained from the DFT + U calculations. In this configuration, $\eta_{\rm IS} \sim 0.7$ $\mu_B$, $\eta_{\rm LS} \sim 0.02$ $\mu_B$, and $\eta_{\rm Fe} \sim 0.03$ $\mu_B$.

the formation of a finite fraction of the IS state configuration (see Fig. S7 in the Supplemental Material [66]) considerably enhancing the magnitude of $M$. One such canted $G_{xy}$ order of the $Co^{3+}$(IS)-$Fe_5^{3+}Co^{3+}$(LS) cluster in the cation disordered structure, as obtained from the DFT + U calculations, is shown Fig. 5. This strongly points at a possible relationship between the JT active $t_{2g}^5 e_g^1$ configuration and the enhancement in the canted magnetization $\mathbf{M}$. However, at this stage, the evidence at our disposal is inadequate. Further investigations are required before one can draw any definite correlation in this regard.

## IV. CONCLUSIONS

We have presented an investigation into the microscopic origins of the experimentally reported canted AFM ($G_{xy}$) order with a net magnetization $\mathbf{M}$ that was formed as a result of substitution of the Fe ions with Co ions in the $R3c$ polar $BiFeO_3$ structure. Our results indicate that in this hexagonal structure, various spin states of the trivalent Co ion energetically compete with each other. This phenomenon was attested by the detection of an electron correlation induced spin crossover transition from LS → HS state configuration. A detailed analysis of our results and their comparative study with the experimental observations indicate towards a simultaneous coexistence of multiple spin states at room temperature. The LS state does not exhibit any particular tendency to stabilize the canted AFM phase. This is sharply in contrast with the behavior of the HS state, which indicates its strong correlation with this particular AFM phase. However, the formation of neither of these spin states leads to any significant enhancement in the magnitude of $\mathbf{M}$. Interestingly, the formation of a finite fraction of an intermediate spin state was found to considerably influence the net magnetization. Therefore, these investigations are expected to initiate further

research for suitable magnetic substitutes in order to enhance the functionalities of this system.

## ACKNOWLEDGMENTS

This work was supported by Grants-in-Aid for Scientific Research No. JP19K05246, No. JP18H05208, No. JP19H05625, and No. JP21K18891, from the Japan Society for the Promotion of Science (JSPS); a Grant-in-Aid for Challenging Research, Organization of Fundamental Research, Tokyo Institute of Technology; and by Design & Engineering by Joint Inverse Innovation for Materials Architecture, MEXT, Japan. We also acknowledge computational support from TSUBAME supercomputing facility.

[1] P. Fischer, M. Polomska, I. Sosnowska, and M. Szymanski, J. Phys. C: Solid State Phys. **13**, 1931 (1980).
[2] C. Ederer and N. A. Spaldin, Phys. Rev. B **71**, 060401(R) (2005).
[3] T. Zhao, A. Scholl, F. Zavaliche, K. Lee, M. Barry, A. Doran, M. P. Cruz, Y. H. Chu, C. Ederer, N. A. Spaldin *et al.*, Nat. Mater. **5**, 823 (2006).
[4] G. Catalan and J. F. Scott, Adv. Mater. **21**, 2463 (2009).
[5] Q. He, C.-H. Yeh, J.-C. Yang, G. Singh-Bhalla, C.-W. Liang, P.-W. Chiu, G. Catalan, L. W. Martin, Y.-H. Chu, J. F. Scott, and R. Ramesh, Phys. Rev. Lett. **108**, 067203 (2012).
[6] J. T. Heron, J. L. Bosse, Q. He, Y. Gao, M. Trassin, L. Ye, J. D. Clarkson, C. Wang, J. Liu, S. Salahuddin *et al.*, Nature (London) **516**, 370 (2014).
[7] D. Lebeugle, D. Colson, A. Forget, and M. Viret, Appl. Phys. Lett. **91**, 022907 (2007).
[8] C. Blaauw and F. Van der Woude, J. Phys. C: Solid State Phys. **6**, 1422 (1973).
[9] S. V. Kiselev, R. P. Ozerov, and G. S. Zhdanov, Sov. Phys. Dokl. **7**, 742 (1963).
[10] I. Sosnowska, T. Peterlin-Neumaier, and E. Steichele, J. Phys. C **15**, 4835 (1982).
[11] M. Ramazanoglu, M. Laver, W. Ratcliff, II, S. M. Watson, W. C. Chen, A. Jackson, K. Kothapalli, S. Lee, S.-W. Cheong, and V. Kiryukhin, Phys. Rev. Lett. **107**, 207206 (2011).
[12] J.-G. Park, M. D. Le, J. Jeong, and S. Lee, J. Phys.: Condens. Matter **26**, 433202 (2014).
[13] I. Gross, W. Akhtar, V. Garcia, L. Martínez, S. Chouaieb, K. Garcia, C. Carrétéro, A. Barthélémy, P. Appel, P. Maletinsky *et al.*, Nature (London) **549**, 252 (2017).
[14] I. Dzyaloshinsky, J. Phys. Chem. Solids **4**, 241 (1958).
[15] T. Moriya, Phys. Rev. **120**, 91 (1960); in *Magnetism I*, edited by G. T. Rado and H. Suhl (Academic Press, New York, 1963), p. 85.
[16] H. Naganuma, J. Miura, and S. Okamura, Appl. Phys. Lett. **93**, 052901 (2008).
[17] I. Coondoo, N. Panwar, A. Tomar, I. Bdikin, A. L. Kholkin, V. S. Puli, and R. S. Katiyar, Thin Solid Films **520**, 6493 (2012).
[18] V. R. Singh, V. K. Verma, K. Ishigami, G. Shibata, Y. Yamazaki, A. Fujimori, Y. Takeda, T. Okane, Y. Saitoh, H. Yamagami *et al.*, J. Appl. Phys. **114**, 103905 (2013).
[19] X. Xue, G. Q. Tan, W. L. Liu, and H. F. Hao, Mater. Lett. **128**, 303 (2014).
[20] K. Shigematsu, T. Asakura, H. Yamamoto, K. Shimizu, M. Katsumata, H. Shimizu, Y. Sakai, H. Hojo, K. Mibu, and M. Azuma, Appl. Phys. Lett. **112**, 192905 (2018).
[21] J. Wang, J. B. Neaton, H. Zheng, V. Nagarajan, S. B. Ogale, B. Liu, D. Viehland, V. Vaithyanathan, D. G. Schlom, U. V. Waghmare *et al.*, Science **299**, 1719 (2003).
[22] F. M. Bai, J. L. Wang, M. Wuttig, J. F. Li, N. G. Wang, A. P. Pyatakov, A. K. Zvezdin, L. E. Cross, and D. Viehland, Appl. Phys. Lett. **86**, 032511 (2005).
[23] S. Ryu, J. Y. Kim, Y. H. Shin, B. G. Park, J. Y. Son, and H. M. Jang, Chem. Mater. **21**, 5050 (2009).
[24] J. Buhot, C. Toulouse, Y. Gallais, A. Sacuto, R. de Sousa, D. Wang, L. Bellaiche, M. Bibes, A. Barthélémy, A. Forget, D. Colson, M. Cazayous, and M.-A. Measson, Phys. Rev. Lett. **115**, 267204 (2015).
[25] A. Agbelele, D. Sando, C. Toulouse, C. Paillard, R. Johnson, R. Rüffer, A. Popkov, C. Carrétéro, P. Rovillain, J.-M. Le Breton *et al.*, Adv. Mater. **29**, 1602327 (2017).
[26] P. Rovillain, R. de Sousa, Y. Gallais, A. Sacuto, M. Méasson, D. Colson, A. Forget, M. Bibes, A. Barthélémy, and M. Cazayous, Nat. Mater. **9**, 975 (2010).
[27] A. F. Popkov, N. E. Kulagin, S. V. Soloviov, K. S. Sukmanova, Z. V. Gareeva, and A. K. Zvezdin, Phys. Rev. B **92**, 140414(R) (2015).
[28] M. Lejman, G. Vaudel, I. C. Infante, P. Gemeiner, V. E. Gusev, B. Dkhil, and P. Ruello, Nat. Commun. **5**, 4301 (2014).
[29] Y. D. Liou, Y. Y. Chiu, R. T. Hart, C. Y. Kuo, Y. L. Huang, Y. C. Wu, R. V. Chopdekar, H. J. Liu, A. Tanaka, C. T. Chen *et al.*, Nat. Mater. **18**, 580 (2019).
[30] J. Gebhardt and A. M. Rappe, Phys. Rev. B **98**, 125202 (2018).
[31] H. Hojo, K. Oka, K. Shimizu, H. Yamamoto, R. Kawabe, and M. Azuma, Adv. Mater. **30**, 1705665 (2018).
[32] I. Sosnowska, M. Azuma, R. Przenioslo, D. Wardecki, W. T. Chen, K. Oka, and Y. Shimakawa, Inorg. Chem. **52**, 13269 (2013).
[33] H. Hojo, R. Kawabe, K. Shimizu, H. Yamamoto, K. Mibu, K. Samanta, T. Saha-Dasgupta, and M. Azuma, Adv. Mater. **29**, 1603131 (2017).
[34] K. Shimizu, R. Kawabe, H. Hojo, H. Shimizu, H. Yamamoto, M. Katsumata, K. Shigematsu, K. Mibu, Y. Kumagai, F. Oba, and M. Azuma, Nano Lett. **19**, 1767 (2019).
[35] H. Yamamoto, T. Kihara, K. Oka, M. Tokunaga, K. Mibu, and M. Azuma, J. Phys. Soc. Jpn. **85**, 064704 (2016).
[36] H. Yamamoto, Y. Sakai, K. Shigematsu, T. Aoyama, T. Kimura, and M. Azuma, Inorg. Chem. **56**, 15171 (2017).
[37] M. Azuma, H. Hojo, K. Oka, H. Yamamoto, K. Shimizu, K. Shigematsu, and Y. Sakai, Annu. Rev. Mater. Res. **51**, 329 (2021).
[38] A. V. Sobolev, V. S. Rusakov, A. M. Gapochka, I. S. Glazkova, T. V. Gubaidulina, M. E. Matsnev, A. A. Belik, and I. A. Presniakov, Phys. Rev. B **101**, 224409 (2020).
[39] K. Shigematsu, H. Shimizu, M. Katsumata, K. Shimizu, H. Yamamoto, K. Mibu, and M. Azuma, Appl. Phys. Express **13**, 071001 (2020).

[40] M. Katsumata, K. Shigematsu, T. Itoh, H. Shimizu, K. Shimizu, and M. Azuma, Appl. Phys. Lett. **119**, 132901 (2021).

[41] T. Itoh, M. Katsumata, K. Shigematsu, and M. Azuma, Appl. Phys. Express **15**, 023002 (2022).

[42] A. Georges, L. d. Medici, and J. Mravlje, Annu. Rev. Condens. Matter Phys. **4**, 137 (2013).

[43] A. Ikeda, Y. H. Matsuda, and K. Sato, Phys. Rev. Lett. **125**, 177202 (2020).

[44] J. Ray, A. K. Biswal, S. Acharya, V. Ganesan, D. K. Pradhan, and P. N. Vishwakarma, J. Magn. Magn. Mater. **324**, 4084 (2012).

[45] V. I. Anisimov, F. Aryasetiawan, and A. Lichtenstein, J. Phys.: Condens. Matter **9**, 767 (1997).

[46] J. P. Perdew, K. Burke, and M. Ernzerhof, Phys. Rev. Lett. **77**, 3865 (1996).

[47] G. Kresse and J. Hafner, Phys. Rev. B **47**, 558(R) (1993).

[48] G. Kresse and J. Furthmiiller, Phys. Rev. B **54**, 11169 (1996).

[49] A. Zunger, S.-H. Wei, L. G. Ferreira, and J. E. Bernard, Phys. Rev. Lett. **65**, 353 (1990).

[50] A. van de Walle, M. Asta, G. Ceder, Calphad **26**, 539 (2002).

[51] P. Blaha, K. Schwarz, G. K. H. Madsen, D. Kvasnicka, J. Luitz, R. Laskowski, F. Tran, and L. D. Marks, *WIEN2k: An Augmented Plane Wave Plus Local Orbitals Program for Calculating Crystal Properties* (Vienna University of Technology, Austria, 2018).

[52] P. Blaha, K. Schwarz, F. Tran, R. Laskowski, G. K. H. Madsen, and L. D. Marks, J. Chem. Phys. **152**, 074101 (2020).

[53] H. J. Monkhorst and J. D. Pack, Phys. Rev. B **13**, 5188 (1976).

[54] N. Metropolis and S. Ulam, J. Am. Stat. Assoc. **44**, 335 (1949).

[55] N. Metropolis, A. W. Rosenbluth, M. N. Rosenbluth, and A. H. Teller, J. Chem. Phys. **21**, 1087 (1953).

[56] C. Ederer and N. A. Spaldin, Phys. Rev. Lett. **95**, 257601 (2005).

[57] R. J. Zeches, M. D. Rossell, J. X. Zhang, A. J. Hatt, Q. He, C.-H. Yang, A. Kumar, C. H. Wang, A. Melville, C. Adamo *et al.*, Science **326**, 977 (2009).

[58] F. Pailloux, M. Couillard, S. Fusil, F. Bruno, W. Saidi, V. Garcia, C. Carrétéro, E. Jacquet, M. Bibes, A. Barthélémy, G. A. Botton, and J. Pacaud, Phys. Rev. B **89**, 104106 (2014).

[59] D. Sando, A. Barthélémy, and M. Bibes, J. Phys.: Condens. Matter **26**, 473201 (2014).

[60] A. A. Belik, S. Iikubo, K. Kodama, N. Igawa, S.-I. Shamoto, S. Niitaka, M. Azuma, Y. Shimakawa, M. Takano, F. Izumi, and E. Takayama-Muromachi, Chem. Mater. **18**, 798 (2006).

[61] H. Ishizaki, H. Yamamoto, T. Nishikubo, Y. Sakai, S. Kawaguchi, K. Yokoyama, Y. Okimoto, S.-Y. Koshihara, T. Yamamoto, and M. Azuma, Inorg. Chem. **58**, 16059 (2019).

[62] Z. Jiang, Y. Nahas, B. Xu, S. Prosandeev, D. Wang, and L. Bellaiche, J. Phys.: Condens. Matter **28**, 475901 (2016).

[63] M. Shaikh, A. Fathima, M. J. Swamynadhan, H. Das, and S. Ghosh, Chem. Mater. **33**, 1594 (2021).

[64] J. M. Rondinelli and N. A. Spaldin, Phys. Rev. B **79**, 054409 (2009).

[65] H. Seo, A. Posadas, and A. A. Demkov, Phys. Rev. B **86**, 014430 (2012).

[66] See Supplemental Material at http://link.aps.org/supplemental/10.1103/PhysRevMaterials.6.064401 for (i) calculated energetics of various spin states of Co ions in the $R3c$ and $P4mm$ phases of $BiCoO_3$ as a function of $U_{\text{eff}}^{\text{Co}}$; (ii) calculated formation energy of the LS, HS and LS+HS configurations of $BiFe_{1-x}Co_xO_3$ compositions; (iii) observed reduction in the volume and the average TM-O (TM → transition metal) bond lengths of the $CoO_6$ octahedra in $BiFe_{1-x}Co_xO_3$ compositions; (iv) calculated net magnetization $M$ of the canted AFM ($G_{xy}$) phase of the parent compound $BiFeO_3$ using Monte Carlo simulations; (v) the critical value of $\mathbf{D}_{xy}^{\gamma}$ at which the transition from the canted AFM $G_{xy}$ → Cycloidal order takes place as a function of in-plane magnetic anisotropy $\alpha$; (vi) the calculated net magnetization $M$ and specific heat as a function of temperature for the $BiFe_{5/6}Co_{1/6}O_3$ HS configurations using Monte Carlo simulations; and (vii) the observed fraction of the intermediate spin (IS) state configuration ($x_{\text{IS}}$) in the mixed spin states.

[67] K. Oka, M. Azuma, W.-T. Chen, H. Yusa, A. A. Belik, E. Takayama-Muromachi, M. Mizumaki, N. Ishimatsu, N. Hiraoka, M. Tsujimoto *et al.*, J. Am. Chem. Soc. **132**, 9438 (2010).

[68] M. Azuma, S. Niitaka, N. Hayashi, K. Oka, M. Takano, H. Funakubo, and Y. Shimakawa, Jpn. J. Appl. Phys. **47**, 7579 (2008).

[69] V. Singh, M. Kosa, K. Majhi, and D. T. Major, J. Chem. Theory Comput. **11**, 64 (2015).

[70] K. Yamauchi, P. Barone, and S. Picozzi, Phys. Rev. B **100**, 245115 (2019).

[71] V. E. Dmitrienko, E. N. Ovchinnikova, S. P. Collins, G. Nisbet, G. Beutier, Y. O. Kvashnin, V. V. Mazurenko, A. I. Lichtenstein, and M. I. Katsnelson, Nature Phys. **10**, 202 (2014).

[72] C. Xu, B. Xu, B. Dupé, and L. Bellaiche, Phys. Rev. B **99**, 104420 (2019).

[73] C. Weingart, N. Spaldin, and E. Bousquet, Phys. Rev. B **86**, 094413 (2012).

[74] M. Matsuda, R. S. Fishman, T. Hong, C. H. Lee, T. Ushiyama, Y. Yanagisawa, Y. Tomioka, and T. Ito, Phys. Rev. Lett. **109**, 067205 (2012).

[75] J. Jeong, E. A. Goremychkin, T. Guidi, K. Nakajima, G. S. Jeon, S.-A. Kim, S. Furukawa, Y. B. Kim, S. Lee, V. Kiryukhin, S.-W. Cheong, and J. G. Park, Phys. Rev. Lett. **108**, 077202 (2012).

[76] Z. Xu, J. Wen, T. Berlijn, P. M. Gehring, C. Stock, M. B. Stone, W. Ku, G. Gu, S. M. Shapiro, R. J. Birgeneau, and G. Xu, Phys. Rev. B **86**, 174419 (2012).

[77] M. Tokunaga, M. Azuma, and Y. Shimakawa, J. Phys. Soc. Jpn. **79**, 064713 (2010).

[78] J. Jeong, M. D. Le, P. Bourges, S. Petit, S. Furukawa, S.-A. Kim, S. Lee, S.-W. Cheong, and J.-G. Park, Phys. Rev. Lett. **113**, 107202 (2014).

[79] R. S. Fishman, J. T. Haraldsen, N. Furukawa, and S. Miyahara, Phys. Rev. B **87**, 134416 (2013).

[80] R. S. Fishman, Phys. B: Condens. Matter **536**, 115 (2018).